

Determination of N^* amplitudes from associated strangeness production in p+p collisions

R. Münzer,^{1,2,*} L. Fabbietti,^{1,2,†} E. Epple,³ S. Lu,² P. Klose,² F. Hauenstein,⁴ N. Herrmann,⁵ D. Grzonka,^{4,6,7} Y. Leifels,⁸ M. Maggiora,⁹ D. Pleiner,² B. Ramstein,¹⁰ J. Ritman,^{4,6,7} E. Roderburg,⁴ P. Salabura,¹¹ A. Sarantsev,¹² Z. Basrak,¹³ P. Buehler,¹⁴ M. Cargnelli,¹⁴ R. Čaplar,¹³ H. Clement,^{15,16} O. Czerwiakowa,¹⁷ I. Deppner,⁵ M. Dželalija,¹⁸ W. Eyrich,¹⁹ Z. Fodor,²⁰ P. Gasik,^{1,2} I. Gašparić,¹³ A. Gillitzer,^{4,6,7} Y. Grishkin,²¹ O.N. Hartmann,⁸ K.D. Hildenbrand,⁸ B. Hong,²² T.I. Kang,^{8,22} J. Kecskemeti,²⁰ Y.J. Kim,⁸ M. Kirejczyk,¹⁷ M. Kiš,⁸ P. Koczon,⁸ R. Kotte,²³ A. Lebedev,²¹ A. Le Fèvre,⁸ J.L. Liu,²⁴ V. Manko,²⁵ J. Marton,¹⁴ T. Matulewicz,¹⁷ K. Piasecki,¹⁷ F. Rami,²⁶ A. Reischl,⁵ M.S. Ryu,²² P. Schmidt,¹⁴ Z. Seres,²⁰ B. Sikora,¹⁷ K.S. Sim,²² K. Siwek-Wilczyńska,¹⁷ V. Smolyankin,²¹ K. Suzuki,¹⁴ Z. Tyimiński,⁵ P. Wagner,²⁶ I. Weber,¹⁸ E. Widmann,¹⁴ K. Wiśniewski,¹⁷ Z.G. Xiao,²⁷ T. Yamasaki,^{28,29} I. Yushmanov,²⁵ P. Wintz,⁴ Y. Zhang,³⁰ A. Zhilin,²¹ V. Zinyuk,⁵ and J. Zmeskal¹⁴

¹Excellence Cluster Universe, Technische Universität München, Boltzmannstr. 2, D-85748, Germany

²Physik Department E62, Technische Universität München, 85748 Garching, Germany

³Yale University, New Haven, Connecticut, United States

⁴Institut für Kernphysik, Forschungszentrum Jülich, 52428 Jülich, Germany

⁵Physikalisches Institut der Universität Heidelberg, Heidelberg, Germany

⁶Jülich Aachen Research Alliance, Forces and Matter Experiments (JARA-FAME)

⁷Experimentalphysik I, Ruhr-Universität Bochum, 44780 Bochum, Germany

⁸GSI Helmholtzzentrum für Schwerionenforschung GmbH, 64291 Darmstadt, Germany

⁹Istituto Nazionale di Fisica Nucleare (INFN) - Sezione di Torino, 10125 Torino, Italy

¹⁰Institut de Physique Nucléaire, CNRS/IN2P3 - Univ. Paris Sud, F-91406 Orsay Cedex, France

¹¹Smoluchowski Institute of Physics, Jagiellonian University of Cracow, 30-059 Kraków, Poland

¹²Petersburg Nuclear Physics Institute, Gatchina, Russia

¹³Ruder Bošković Institute, Zagreb, Croatia

¹⁴Stefan-Meyer-Institut für subatomare Physik, Österreichische Akademie der Wissenschaften, Wien, Austria

¹⁵Physikalisches Institut der Universität Tübingen,

Auf der Morgenstelle 14, 72076 Tübingen, Germany

¹⁶Kepler Center for Astro and Particle Physics, University of Tübingen,

Auf der Morgenstelle 14, 72076 Tübingen, Germany

¹⁷Institute of Experimental Physics, Faculty of Physics, University of Warsaw, Warsaw, Poland

¹⁸Faculty of Science, University of Split, Split, Croatia

¹⁹Friedrich-Alexander-Universität Erlangen-Nürnberg, 91058 Erlangen, Germany

²⁰Wigner RCP, RMKI, Budapest, Hungary

²¹Institute for Theoretical and Experimental Physics, Moscow, Russia

²²Korea University, Seoul, Korea

²³Institut für Strahlenphysik, Helmholtz-Zentrum Dresden-Rossendorf, Dresden, Germany

²⁴Harbin Institute of Technology, Harbin, China

²⁵National Research Centre 'Kurchatov Institute', Moscow, Russia

²⁶Institut Pluridisciplinaire Hubert Curien and Université de Strasbourg, Strasbourg, France

²⁷Department of Physics, Tsinghua University, Beijing, China

²⁸Department of Physics, The University of Tokyo, Tokyo, 113-0033

²⁹RIKEN Nishina Center, RIKEN, Wako, 351-0198, Japan

³⁰Institute of Modern Physics, Chinese Academy of Sciences, Lanzhou, China

We present the first determination of the energy-dependent production amplitudes of N^* resonances with masses between 1650 MeV/ c^2 and 1900 MeV/ c^2 for an excess energy between 0 and 600 MeV. A combined Partial Wave Analysis of seven exclusively reconstructed data samples for the reaction $p+p \rightarrow pK^+\Lambda$ measured by the COSY-TOF, DISTO, FOPI and HADES collaborations in fixed target experiments at kinetic energies between 2.14 and 3.5 GeV is used to determine the amplitude of the resonant and non-resonant contributions.

Keywords: partial wave analysis, resonance, hadrons, strangeness, scattering length, hyperon-nucleon interaction

A quantitative understanding of the role played by baryonic resonances in nucleon-nucleon reactions at kinetic energies of a few GeV [1–8] is important for the study of dilepton and hadron production in elementary and heavy ion collisions [9]. Most of the analyses of

nucleus-nucleus collisions that study dilepton and hadron production published so far in both sectors considered at most incoherent cocktails of contributing sources that eventually also included resonances to describe the measured spectra [10, 11]. For final states containing pions

and nucleons produced in elementary reactions partial wave analysis (PWA) was already employed to correctly take into account interferences and determine the amplitude of the contributing waves [12–15].

The N^* decay into open strangeness ($N^* \rightarrow K + \Lambda$) was first studied by analyzing the Dalitz plot for the reaction $p + p \rightarrow p + K^+ + \Lambda$ up to kinetic energies of $T = 2.5$ GeV, but without accounting for interference effects [8]. The HADES collaboration has employed a PWA for the search for the kaonic bound state ppK^- [17, 18] in the reaction $p + p \rightarrow p + K^+ + \Lambda$ at a beam kinetic energy of 3.5 GeV. In this reaction the N^* contribute to the measured final state and influence the background for the kaonic bound state [16, 19]. It was shown in Ref. [16] that the PWA is able to reproduce the experimental data by the coherent sum of the different N^* and the non-resonant $pK^+ \Lambda$ final states without introduction of the exotic state ppK^- . The existence of the ppK^- can however not be excluded since the extracted upper limits are in the order of few μb . This method was further improved by developing a framework that allows for the simultaneous analysis of seven different data sets measured by the COSY-TOF, HADES, DISTO and FOPI experiments. The reaction $p + p \rightarrow p + K^+ + \Lambda$ was measured in fixed target experiments at kinetic energies varying from 2.14 to 3.5 GeV [16, 20–25]. This way, the energy-dependent amplitude of seven different contributing N^* resonances decaying into the Λ - K^+ channel and of non-resonant $pK^+ \Lambda$ final states could be extracted for the first time.

A second interesting aspect is the study of the $p\Lambda$ interaction. This interaction was previously investigated primarily by means of scattering experiments [26–28]. The reaction $p + p \rightarrow p + K^+ + \Lambda$ offers the possibility to study the final state interaction of the p - Λ pair as an alternative to scattering experiments [25, 28–30]. Since so far the resonances were not treated in a coherent way, a precise determination of their contributions and of the scattering lengths and effective ranges is challenging. The combined PWA presented in this work offers the unique possibility to study the interplay between the N^* coupling to the Λ - K^+ channel and the p - Λ final state interaction. The experimental data were measured by the COSY-TOF, DISTO, FOPI and HADES collaborations. Table I contains an overview of the data sets used for the combined PWA, their beam energy and the available statistics. Together with the each experimental data set, simulations of the $pK^+ \Lambda$ production according to phase space kinematics, filtered through the detector and analysis selections are used for the PWA. The details about the reconstruction of the exclusive $pK^+ \Lambda$ final state, achieved resolution, efficiency, and purity are explained in the already published works by the different collaborations [16, 20–25]. The two HADES data samples at the same kinetic energy correspond to two different reconstruction analyses including or excluding the forward spectrometer [16].

The goal of this PWA is to employ the seven data samples in a combined analysis and extract the amplitudes of the different waves, characterised by their quantum numbers, leading to given final states. We use the Bonn-Gatchina PWA (BG-PWA) framework [13, 14] to fit event-by-event the measured 4-momenta for the exclusive final state $p + p \rightarrow p + K^+ + \Lambda$ weighted with the coherent superposition of specific participating waves. The best choice for the waves used in the PWA is determined by comparing the experimental data to the PWA output event-by-event in terms of a log-likelihood parameter. In the specific case of the COSY-TOF data sample, only the region of phase space within $|\cos \theta_{\text{cms},p}| < 0.7$ was considered because of the poor description of the trigger efficiency in the simulation for the excluded region. For the DISTO data samples the region corresponding to $\cos \theta_{\text{cms},p} > 0.95$ was excluded from the fit to minimize the bias introduced by the digitization of the scintillation-fiber sub detector used for tracking close to the target region.

The formalism adopted within the BG-PWA to parametrize resonant and non-resonant waves is explained in detail in Refs. [12, 16]. The same parametrization was adopted in this global analysis with a single exception: the parametrization of the transition amplitude shown there, that is suited for the analysis of a single data set at a fixed kinetic energy, was replaced by the energy-dependent amplitude as described in Refs. [13, 14]. For the analysis presented here, the N^* resonances listed in Table II have been considered with masses and widths taken from [31, 32]. This choice is motivated by the expected branching ratio into the $K\Lambda$ channel. Constant masses and widths have been assumed in the PWA for all the resonances. For the non-resonant case, the effective range approximation is used and the amplitude is parametrized as in Ref. [16], Eq. (5). The values of the scattering length and effective range for the $p\Lambda$ pair in s-wave can be set as free parameters in the PWA fit and hence be extracted within this analysis.

Another intermediate channel contributing to the $pK^+ \Lambda$ final state is the Σ - N cusp, which appears at or above the p - Σ threshold (2.13 GeV/ c^2) [33]. The coupling between the Σ - N and Λ - N channels leads to an enhancement of the cross section in the p - Λ final state in a mass range close to the above mentioned threshold. Due to the virtual character of the intermediate Σ - N state, this channel interferes with the other production channels. In order to include the cusp contribution in the BG-PWA framework, new transition waves have been added. Since the production via this channel happens directly at threshold, the Σ and N are expected to be in a relative s-wave state, which means that the spin-parity of the Σ - N system is either $J^P = 0^+$ or 1^+ [33]. The resulting p - Λ system is then an s-wave state, in case of $J^P = 0^+$, or an s- or d-wave state in case of $J^P = 1^+$, which has also been confirmed through an analysis of the Σ - N cusp carried out by the COSY-TOF collaboration [33]. The three cusp waves

TABLE I. List of available statistics for the reaction $p+p \rightarrow p+K^+\Lambda$ measured by the COSY-TOF, DISTO, FOPI and HADES collaborations. The kinetic beam energy, the total cross section and the reduced χ^2 values resulting from different PWA analyses are shown (see text for details).

experiment	T (GeV)	statistics	σ_{tot} [mb]	$\chi^2/ndf(\text{single})$	$\chi^2/ndf(\text{combined})$
DISTO [20, 21]	2.14	121000	19.0 ± 3.3	0.52	1.52
COSY-TOF -TOF [23, 25]	2.16	43662	19.7 ± 3.5	1.69	0.44
DISTO [20, 21]	2.5	304000	30.5 ± 5.7	2.85	2.56
DISTO [20–22]	2.85	424000	38.7 ± 7.9	7.68	3.55
FOPI [24]	3.1	903	43.1 ± 9.3	1.21	0.91
HADES [16]	3.50	13155	48.0 ± 11.5	1.12	2.14
HADES [16]	3.50	8155	48.0 ± 11.5	1.38	1.86

TABLE II. N^* resonances included in the PWA written in the spectroscopic notation with the corresponding masses, widths and branching ratios in the $K\Lambda$ final states [31, 32].

N^*	J^P	Mass ($\frac{\text{GeV}}{c^2}$)	Width ($\frac{\text{GeV}}{c^2}$)	$\Gamma_{K\Lambda}/\Gamma_{tot}$ (%)
1650	$\frac{1}{2}^-$	1.655	0.15	7 ± 4
1710	$\frac{1}{2}^+$	1.710	0.20	15 ± 10
1720	$\frac{3}{2}^+$	1.720	0.25	8 ± 7
1875	$\frac{3}{2}^-$	1.875	0.20	4 ± 2
1880	$\frac{1}{2}^+$	1.870	0.25	2 ± 1
1895	$\frac{1}{2}^-$	1.895	0.09	18 ± 5
1900	$\frac{3}{2}^+$	1.900	0.26	5 ± 5

have been included to the BG-PWA. The same Breit-Wigner parametrization was employed as for the N^* and the mass and width of the cusp resonance were varied between $2.1 - 2.16 \text{ GeV}/c^2$ and $0.01 - 0.03 \text{ GeV}/c^2$, respectively.

First, the PWA was performed individually for the different data samples to determine the correct start values of the parameters for the global fit. The best solution corresponds to the minimum of the log-likelihood obtained by fitting the experimental data with the PWA event-by-event.

A comparison of the three missing mass spectra and CMS, Gottfried-Jackson and Helicity angle distributions (for the definition of these variables see [6]) obtained from the experimental data and from the single PWA fits was carried out and the corresponding reduced χ^2 values are listed in Table I. As a second step, a simultaneous PWA of three data samples was carried out. This intermediate step allowed to determine the starting values for the global fit. The HADES, FOPI and DISTO ($T = 2.5 \text{ GeV}$) samples were selected to account for both the contributions from the Σ -N cusp and from higher mass resonances. After finding a solution that described the three data samples, further data samples were added

stepwise. The starting values of each new PWA fit were taken from the results of the previous fit step. Systematic studies were carried out by considering all permutations for the exclusion of one or more N^* resonances from the list in Table II. The five best solutions in terms of log-likelihood obtained from these systematic variation of the PWA fits were considered to extract the final results and the PWA systematic errors. As far as the resonances are concerned, considering the list of seven resonances in Table II, the five best solutions correspond to the following combinations: 1) all seven N^* included, 2) $N^*(1720)$ excluded, 3) $N^*(1875)$ excluded, 4) $N^*(1900)$ excluded and, 5) $N^*(1900)$ and $N^*(1875)$ excluded.

The reduced χ^2 values for the combined PWA listed in Table I were obtained by comparing the experimental data in the mass and angle variables with the average values of the five best PWA solutions, taking as errors the statistical errors of the experimental data and the standard deviation of the five solutions for each bin.

Figure 1 shows the missing mass distributions (MM) for the three final state particles p , Λ and K^+ for COSY-TOF at 2.16 GeV (blue symbols), DISTO at 2.85 GeV (green symbols) and HADES at 3.5 GeV (red symbols) data samples measured within their respective acceptances and arbitrarily normalized. The signature of the Σ -N cusp is visible in the COSY-TOF and DISTO MM_{K^+} around $2.13 \text{ GeV}/c^2$. The errors of the experimental data are statistical only. The lines in the same color-code represent the PWA results for the corresponding data sets. The line widths represent the error bands of the global PWA fit expressed as the standard deviation of the five best PWA solutions. A similar quality for the description of the kinematic variables obtained with the global PWA is of similar quality as compared to other data samples. The output of each PWA solution provides the strength of the individual waves with respect to the total measured yield. The resulting relative contributions of the resonant and non-resonant waves can be translated into cross sections for the $K\Lambda$ decay channel by normalizing the relative yield to the total production cross section for

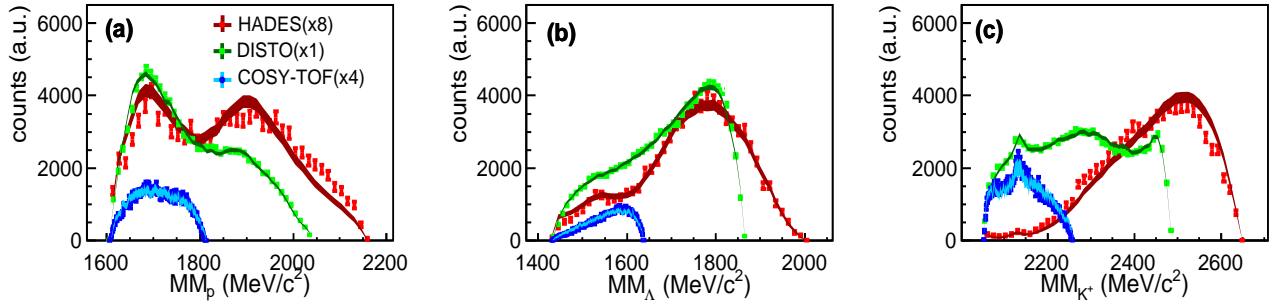


FIG. 1. (Color online). Missing mass distributions (MM) for the three different particles of the final state (p, Λ , K^+) are shown. The experimental data within the geometrical acceptance are from COSY-TOF at 2.16 GeV (blue symbols), DISTO at 2.85 GeV (green symbols) and HADES at 3.5 GeV (red symbols) samples. The colored lines in the same color-code represent the PWA results (see text for details).

the $pK^+\Lambda$ final state.

The total $pK^+\Lambda$ cross section for the different data sets was evaluated employing a phase space fit of the existing measurements of the $pK^+\Lambda$ channel as a function of the excess energies [8, 23, 33–35]. The error associated to the $pK^+\Lambda$ cross section of each data sample is extracted from the fit. A detailed description of the extraction of the $pK^+\Lambda$ cross sections can be found in [36].

In Figure 2 the cross section for the different N^* channels decaying into the $K\Lambda$ final state is plotted versus its excess energy. The standard deviation of the five best solutions is shown by the black vertical error bars, the green bands show the error originating from the cross section normalization (see Table II). The non-vanishing cross section below the respective thresholds is due to the large width of all the considered resonances (see Table II). The relative contribution of the non-resonant amplitude decreases from 37% for 2.14 GeV to 10% for 3.5 GeV, so that most of the yield stems from N^* resonances for all the measured energies. The dominant contribution by the N^* resonances is consistent with the results shown in Ref. [8], except for the relative contribution of the $N^*(1650)$, which is decreasing as a function of the beam energy in [8]. In this work we found an increment of the $N^*(1650)$ similarly to the $N^*(1710)$ and $N^*(1720)$. This difference probably results from the neglect of interference in Ref. [8].

The Σ -N cusp contribution varies from 10^{-3} to 10^{-2} with decreasing energy with respect to the N^* and is not shown in Figure 2. The global PWA fit favors the Σ -N cusp contribution of the s- or d-wave state $J^P = 1^+$ with respect to the s-wave $J^P = 0^+$. The obtained Σ -N cusp yield is slightly different from the findings in Ref. [33] where at a beam energy of 2.28 GeV the contribution of the cusp was found equal to 5% of the total cross section, but neglecting interferences.

Figure 3 shows the amplitude of the different p+p initial states as a function of the $pK^+\Lambda$ excess energy. The error bars are associated to the standard deviation of the

five best PWA solutions, and the green band refers to the uncertainty of the inclusive $pK^+\Lambda$ production cross section.

The non-resonant amplitude included in this PWA is parametrized as a function of the scattering length and effective range for the p- Λ final state interaction. This way, the values for s-wave singlet and s-wave triplet can be extracted independently. In Table III the resulting values are listed. The values are obtained by averaging the five best PWA solutions. The first error represents the standard deviation of the five fit results. The second one is the PWA fit error obtained by adding quadratically the PWA fit errors from the five solutions. In the same table also the scattering lengths and effective ranges obtained from p+p reactions with unpolarized [28, 37] and polarized beams [29] are shown.

The results from this PWA are compatible with some of previously extracted values. A reanalysis of the data samples with the lower kinetic energy is necessary to limit the contribution by angular momenta higher than s-wave in the non resonant amplitude and extract more conclusive results on the p- Λ scattering parameters.

* robert.muenzer@cern.ch

† laura.fabbietti@ph.tum.de

- [1] V. P. Andreev et al., Phys. Rev. **C50**, 15 (1994).
- [2] V. Sarantsev et al., Eur. Phys. J. **A21**, 303 (2004).
- [3] G. Agakishiev et al., Phys. Lett. **B750**, 184 (2015).
- [4] L. Fabbietti et al., Nucl. Phys. **A914**, 60 (2013).
- [5] G. Agakishiev et al., Phys. Rev. **C87**, 025201 (2013).
- [6] G. Agakishiev et al., Phys. Rev. **C85**, 035203 (2012).
- [7] G. Agakishiev et al., Phys. Rev. **C90**, 015202 (2014).
- [8] S. Abd El-Samad et al., Phys. Lett. **B688**, 142 (2010).
- [9] G. Agakishiev et al., Phys. Rev. **C84**, 014902 (2011).
- [10] G. Agakishiev et al., Eur. Phys. J. **A50**, 82 (2014).
- [11] J. Weil and U. Mosel, EPJ Web Conf. **52**, 06007 (2013).
- [12] G. Agakishiev et al., Eur. Phys. J. **51**, 137 (2015).

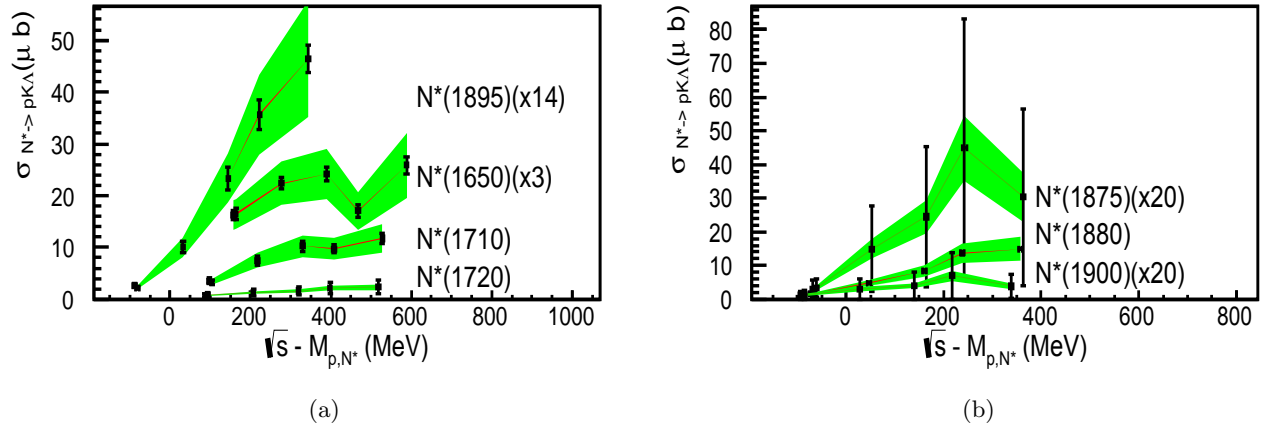


FIG. 2. (Color online). Amplitudes of the different N^* resonances decaying into the $pK^+\Lambda$ final state obtained from the combined PWA as a function of the excess energy. The black bars show the systematic errors originating from the five different PWA solutions and the green bands represent the errors due to the normalization to the total $pK^+\Lambda$ cross section.

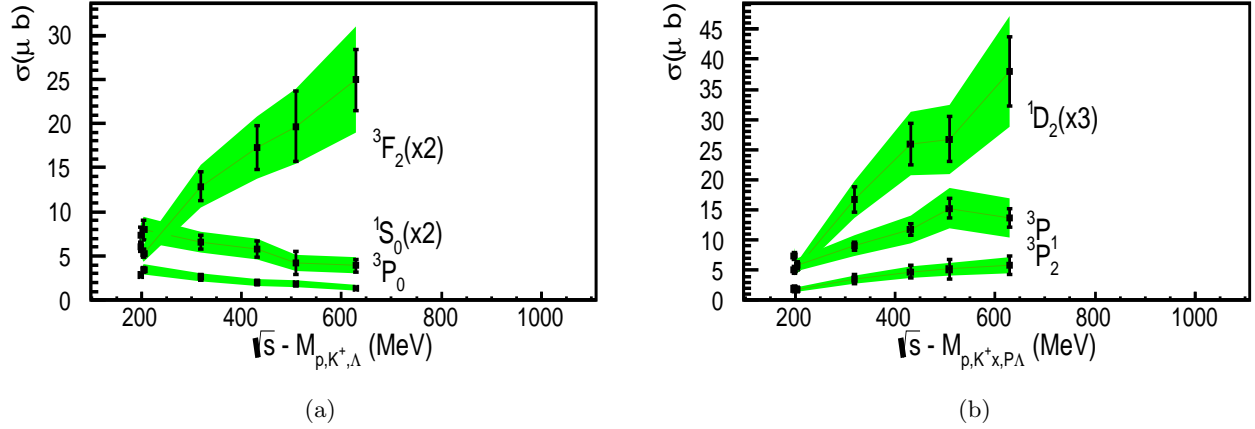


FIG. 3. (Color online). Amplitude of the initial state waves as a function of the excess energy for the $pK^+\Lambda$ final state. The error bars correspond to the standard deviation among the five best PWA solutions and the green band refers to the normalization to the total $pK^+\Lambda$ production cross section.

- [13] A. V. Anisovich and A. V. Sarantsev, Eur. Phys. J. **A30**, 427 (2006).
- [14] A. V. Anisovich, V. V. Anisovich, E. Klempt, V. A. Nikonov, and A. V. Sarantsev, Eur. Phys. J. **A34**, 129 (2007).
- [15] K. N. Ermakov, V. I. Medvedev, V. A. Nikonov, O. V. Rogachevsky, A. V. Sarantsev, V. V. Sarantsev, and S. G. Sherman, Eur. Phys. J. **A50**, 98 (2014).
- [16] G. Agakishiev et al., Phys. Lett. **B742**, 242 (2015).
- [17] T. Yamazaki and Y. Akaishi, Physics Letters B **535**, 70 (2002).
- [18] T. Yamazaki et al., Phys. Rev. Lett. **104**, 132502 (2010).
- [19] E. Eppe and L. Fabbietti, Phys. Rev. **C92**, 044002 (2015).
- [20] M. Maggiora et al., Nucl. Phys. **A835**, 43 (2010).
- [21] M. Maggiora, Nucl. Phys. **A691**, 329 (2001).
- [22] F. Balestra et al., Phys. Rev. Lett. **83**, 1534 (1999).
- [23] M. Abdel-Bary et al., Eur. Phys. J. **A46**, 27 (2010).
- [24] R. Münzer, Dissertation, TU München (2014).
- [25] M. Röder et al., Eur. Phys. J. **A49**, 157 (2013).
- [26] B. Sechi-Zörn, B. Kehoe, J. Twitty, and R. A. Burnstein, Phys. Rev. **175**, 1735 (1968).
- [27] F. Eisele, H. Filthuth, W. Föhlisch, V. Hepp, and G. Zech, Phys. Lett. **B37**, 204 (1971).
- [28] G. Alexander et al., Phys. Rev. **173**, 1452 (1968).
- [29] F. Hauenstein et al., PRC in print (2016), arXiv:1607.04783 [nucl-ex].
- [30] J. Adamczewski-Musch et al., Phys. Rev. C **94** (2016).
- [31] J. Beringer et al., Phys. Rev. **D86**, 010001 (2012).
- [32] A. V. Anisovich et al., Eur. Phys. J. **A48**, 15 (2012).
- [33] S. Abd El-Samad et al., Eur. Phys. J. **A49**, 41 (2013).
- [34] S. Abdel-Samad et al., Phys. Lett. **B632**, 27 (2006).
- [35] W. G. M. A. Baldini, V. Flaminio and D. R. O. Morrison, in Landolt-Börnstein, New Series, Subvolume a and b (Springer-Verlag, Heidelberg, 1985) p. 417(a) and 468(b).
- [36] R. Muenzer et al., arXiv:1610.03678 [nucl-ex].
- [37] A. Budzanowski et al., Phys. Lett. **B687**, 31 (2010).

TABLE III. Scattering length and effective range extracted from the combined PWA fit and reference values from theoretical calculation and previous measurement (see text for details).

Source	1S_0 $a_{\Lambda-p}$ [fm]	1S_0 $r_{\Lambda-p}$ [fm]	3S_1 $a_{\Lambda-p}$ [fm]	3S_1 $r_{\Lambda-p}$ [fm]
This work	$-1.43 \pm 0.36 \pm 0.09$	$1.31 \pm 0.24 \pm 0.16$	$-1.88 \pm 0.38 \pm 0.10$	$1.04 \pm 0.78 \pm 0.15$
[28]	$-1.8^{+2.3}_{-4.2}$	-	$-1.6^{+1.1}_{-0.8}$	-
[37]	$-2.43^{+0.16}_{-0.25}$	$2.21^{+0.16}_{-0.36}$	$-1.56^{+0.19}_{-0.22}$	$3.7^{+0.6}_{-0.6}$
[29]	-	-	$-2.55^{+0.72}_{-1.39} \pm 0.6 \pm 0.3$	-

TABLE IV. Production cross sections of the total $pK^+\Lambda$ non-resonant contribution and of the different N^* resonances decaying into the $pK^+\Lambda$ final state obtained from the global PWA as a function of the beam kinetic energy. The cross sections refer to the amplitudes prior to the coherent sum of the latter and hence do not consider interference effects. The N^* cross sections are not corrected for the branching ratio into the $K^+\Lambda$ final states. The first error corresponds to the systematic error due to the five best solutions, the second stems from the cross section normalisations. The systematic error of the PWA fitting procedure is found to be negligible and hence is not shown.

	3.500 GeV	3.100 GeV	2.85 GeV
$pK^+\Lambda$ [μb]	$5.1 \pm 1.0 \pm 1.2$	$6.3 \pm 1.2 \pm 1.4$	$6.5 \pm 1.1 \pm 1.3$
$N^*(1650) \rightarrow pK^+\Lambda$ [μb]	$8.6 \pm 0.6 \pm 2.1$	$5.7 \pm 0.4 \pm 1.2$	$8.1 \pm 0.4 \pm 1.6$
$N^*(1710) \rightarrow pK^+\Lambda$ [μb]	$11.7 \pm 1.0 \pm 2.8$	$9.7 \pm 0.8 \pm 2.1$	$10.2 \pm 1.0 \pm 2.1$
$N^*(1720) \rightarrow pK^+\Lambda$ [μb]	$2.4 \pm 1.3 \pm 0.6$	$2.2 \pm 1.2 \pm 0.5$	$1.6 \pm 0.8 \pm 0.3$
$N^*(1875) \rightarrow pK^+\Lambda$ [μb]	$1.5 \pm 1.3 \pm 0.4$	$2.2 \pm 1.9 \pm 0.5$	$1.2 \pm 1.0 \pm 0.2$
$N^*(1880) \rightarrow pK^+\Lambda$ [μb]	$14.9 \pm 0.2 \pm 3.6$	$13.7 \pm 0.4 \pm 3.0$	$8.4 \pm 0.4 \pm 1.7$
$N^*(1895) \rightarrow pK^+\Lambda$ [μb]	$3.3 \pm 0.2 \pm 0.8$	$2.5 \pm 0.2 \pm 0.6$	$1.7 \pm 0.2 \pm 0.3$
$N^*(1900) \rightarrow pK^+\Lambda$ [μb]	$0.2 \pm 0.2 \pm 0.0$	$0.3 \pm 0.3 \pm 0.1$	$0.2 \pm 0.2 \pm 0.0$
$\Sigma-N(1^+S)$ [μb]	$0.01 \pm 0.02 \pm 0.002$	$0.03 \pm 0.02 \pm 0.007$	$0.12 \pm 0.05 \pm 0.02$
$\Sigma-N(1^+D)$ [μb]	$0.13 \pm 0.02 \pm 0.03$	$0.2 \pm 0.04 \pm 0.05$	$0.5 \pm 0.08 \pm 0.1$
	2.5 GeV	2.157 GeV	2.14 GeV
$pK^+\Lambda$ [μb]	$7.2 \pm 1.1 \pm 1.3$	$7.5 \pm 0.6 \pm 1.3$	$7.1 \pm 0.6 \pm 1.2$
$N^*(1650) \rightarrow pK^+\Lambda$ [μb]	$7.5 \pm 0.4 \pm 1.4$	$5.5 \pm 0.3 \pm 1.0$	$5.4 \pm 0.3 \pm 1.0$
$N^*(1710) \rightarrow pK^+\Lambda$ [μb]	$7.5 \pm 0.9 \pm 1.4$	$3.3 \pm 0.5 \pm 0.6$	$3.5 \pm 0.5 \pm 0.6$
$N^*(1720) \rightarrow pK^+\Lambda$ [μb]	$1.3 \pm 0.7 \pm 0.2$	$0.8 \pm 0.4 \pm 0.1$	$0.7 \pm 0.3 \pm 0.1$
$N^*(1875) \rightarrow pK^+\Lambda$ [μb]	$0.7 \pm 0.6 \pm 0.1$	$0.2 \pm 0.1 \pm 0.0$	$0.2 \pm 0.1 \pm 0.0$
$N^*(1880) \rightarrow pK^+\Lambda$ [μb]	$4.8 \pm 0.3 \pm 0.9$	$1.7 \pm 0.1 \pm 0.3$	$1.5 \pm 0.1 \pm 0.3$
$N^*(1895) \rightarrow pK^+\Lambda$ [μb]	$0.7 \pm 0.1 \pm 0.1$	$0.2 \pm 0.0 \pm 0.0$	$0.2 \pm 0.0 \pm 0.0$
$N^*(1900) \rightarrow pK^+\Lambda$ [μb]	$0.2 \pm 0.2 \pm 0.0$	$0.1 \pm 0.1 \pm 0.0$	$0.1 \pm 0.1 \pm 0.0$
$\Sigma-N(1^+S)$ [μb]	$0.12 \pm 0.04 \pm 0.02$	$0.16 \pm 0.04 \pm 0.03$	$0.13 \pm 0.03 \pm 0.02$
$\Sigma-N(1^+D)$ [μb]	$0.34 \pm 0.07 \pm 0.06$	$0.21 \pm 0.04 \pm 0.04$	$0.17 \pm 0.03 \pm 0.03$

TABLE V. Contributions of the different initial state waves as a function of the beam kinetic energy. The obtained cross sections are normalised to the inclusive $pK^+\Lambda$ cross section. The first error corresponds to the systematic error due to the five best solutions, the second originates from the cross section normalisation. The systematic error of the PWA fitting procedure is found to be negligible and hence is not shown.

	3.5 GeV	3.1 GeV	2.85 GeV	2.5 GeV	2.157 GeV	2.140 GeV
$\sigma_{pK\Lambda}$ [μb]	48.0 ± 5.8	43.1 ± 5.3	38.7 ± 4.8	30.5 ± 3.9	19.7 ± 2.7	19.0 ± 2.6
1S_0 [μb]	$2.0 \pm 0.4 \pm 0.5$	$2.1 \pm 0.6 \pm 0.5$	$2.9 \pm 0.5 \pm 0.6$	$3.3 \pm 0.4 \pm 0.6$	$4.0 \pm 0.6 \pm 0.7$	$3.7 \pm 0.5 \pm 0.6$
1D_2 [μb]	$12.7 \pm 1.9 \pm 3.0$	$8.9 \pm 1.2 \pm 1.9$	$8.6 \pm 1.2 \pm 1.8$	$5.6 \pm 0.7 \pm 1.0$	$1.8 \pm 0.1 \pm 0.3$	$2.5 \pm 0.2 \pm 0.4$
3P_0 [μb]	$1.4 \pm 0.2 \pm 0.3$	$1.8 \pm 0.2 \pm 0.4$	$2.1 \pm 0.3 \pm 0.4$	$2.6 \pm 0.3 \pm 0.5$	$3.5 \pm 0.3 \pm 0.6$	$2.9 \pm 0.2 \pm 0.5$
3P_1 [μb]	$13.7 \pm 1.4 \pm 3.3$	$15.3 \pm 1.6 \pm 3.3$	$11.8 \pm 0.9 \pm 2.4$	$9.1 \pm 0.7 \pm 1.7$	$5.9 \pm 0.6 \pm 1.0$	$5.1 \pm 0.5 \pm 0.9$
3P_2 [μb]	$5.8 \pm 1.5 \pm 1.4$	$5.2 \pm 1.5 \pm 1.1$	$4.8 \pm 1.1 \pm 1.0$	$3.5 \pm 0.8 \pm 0.7$	$1.8 \pm 0.4 \pm 0.3$	$1.9 \pm 0.4 \pm 0.3$
3F_2 [μb]	$12.5 \pm 1.7 \pm 3.0$	$9.8 \pm 2.0 \pm 2.1$	$8.6 \pm 1.2 \pm 1.8$	$6.4 \pm 0.8 \pm 1.2$	$2.7 \pm 0.3 \pm 0.5$	$3.0 \pm 0.3 \pm 0.5$